Qeios

Seismic intensity measure selection considering Record-to-Record and Angle-to-Angle uncertainties.

Reza Barati[1]*, Ghasem Boshrouei Shargh[2]

1.Department of Civil Engineering, Ferdowsi University of Mashhad, Iran, *reza.barati@alumni.um.ac.ir*
2. Department of Architectural Engineering, The Pennsylvania State University, University Park, State College, PA, USA

Abstract

This study addresses the critical task of selecting an appropriate seismic intensity measure to assess structural performance under earthquake loading. It explores the impact of intensity measure selection on two significant sources of uncertainty: Record-to-Record (R-to-R) and Angle-to-Angle (A-to-A) variability. While R-to-R variability has been extensively studied, A-to-A variability remains relatively unexplored. A large set of Intensity Measures are evaluated and compared in terms of their Record-to-Record Efficiency and Angular Efficiency. This study aims to provide a more comprehensive understanding of their suitability, regarding the simultaneous impact of mentioned uncertainties. Numerical analyses are conducted on two moment-resisting steel frame structures subjected to a diverse set of ground motions along with ten rotation angles. The efficiency of different intensity measures is computed, among which E_v indicated an acceptable performance in reducing the parallel randomness in probabilistic seismic performance assessment.

Keywords: Rotation angle, Angle-to-Angle variability, Angular efficiency, Ground motion intensity measures, Probabilistic seismic demand model, Relative entropy

1- Introduction

Understanding the natural uncertainty involved in the earthquake's impact on the structures calls for probabilistic methods that can accommodate various sources of uncertainty. The well-established *PEER* framework (Moehle et al., 2004) has been able to meet this need by utilizing the total probability rule, which accounts for different known effects simultaneously. This approach necessitates choosing an appropriate seismic intensity measure (IM) as a representative of the ground shaking phenomenon linking its characteristics to structural properties. For this purpose, during the last two decades, many studies have been carried out by researchers focusing on choosing the most appropriate measure of seismic intensity.

A competent measure of ground motion intensity is expected to capture a wide range of uncertainty such as *Record-to-Record* (R-to-R) and *Angle-to-Angle* (A-to-A) variability. Record-to-record variability refers to different responses of a structure under different input waveforms at the same level of intensity, or when the intensity levels vary but the responses are not linearly proportional to them,

which largely depends on the R-to-R efficiency of the employed intensity measure. Also, the angle-to-angle variability pertains to structural response variation under different recording angles of the same ground motion, which is caused by the randomness in the recording process. While the former has been extensively studied, the latter remains relatively understudied. Boshrouei Sharg and Barati (Shargh et al., 2023) studied *angle-to-angle* variability by examining two 3- and 9-story steel bending frame structures, and the result has shown the obvious impact of this random phenomenon on structural performance. However, the focus of the mentioned research was only on a single Intensity Measure (*IM*), the spectral acceleration of the first mode of the structure $S_a(T_1)$. It has been shown that the selection of a more appropriate seismic intensity measure can reduce the inherent uncertainty of *R-to-R* variability (Luco et al., 2007). Thus, it is worth investigating the impact of this choice on the level of uncertainty induced by *A-to-A* variability. In this regard, (Shargh et al., 2024) proposed the concept of *Angular Efficiency* to quantify the effect of *IM* selection on the *angle-to-angle* variability. However, the simultaneous effects of both mentioned sources of uncertainty on this selection are yet to be explored. To this end, the current study aims to provide a method to address this, creating a more comprehensive approach to studying the *Efficiency* and *Angular Efficiency* of different *IMs*. To study the various intensity measures, two 3- and 9-story moment-resisting steel frame structures each under 100 ground motions at 10 different recording angles are analyzed (1000 nonlinear time history analyses for each structure). Utilizing two numerical criteria representing the mentioned variabilities, a set of *Intensity Measures* is evaluated and compared.

2- Uncertainty of ground motion rotation

The recorded history of earthquake acceleration is essential for achieving a realistic understanding of earthquake waveform and its impacts. By examining the recording process during seismic events, one can detect the uncertainties related to the ground motion recording angle. This uncertainty stems from capturing the two horizontal components of the earthquake acceleration history in predetermined directions by the accelerometer. In other words, the two recorded horizontal components after the earthquake depend on the two geographical directions where the sensors of the device were set before the event. Thus, if the device's sensors were different from the determined directions, the recorded acceleration history would have been altered, leading to a varied response in the structure.

It was previously shown by the authors of this study (Shargh et al., 2023) that the mentioned impact is not ignorable. To account for this impact, one needs to conduct nonlinear analyses to evaluate the seismic performance of the structure in various rotation angles. However, as an optimal solution, in the same study, it was shown that employing the ground acceleration history associated with the median value of $S_a(T_1)$ can provide adequate accuracy without increasing the number of analyses.

Also, to quantify the A-to-A variability, in another research by the authors (Shargh et al., 2024), a criterion called *Angular Efficiency* has been introduced, which quantifies this uncertainty for a given *IM* and structure. The current study aims to quantify the record-to-record and angle-to-angle uncertainty concurrently to assess the versatility of different intensity measures to facilitate the process of choosing the optimal intensity measure. Given a pair of ground acceleration histories, the acceleration corresponding to angle θ can be calculated using the Eq. (1):

$$a_\theta = \cos\theta.a_x + \sin\theta.a_y \quad (1)$$

Herein, ax and ay are the ground motion acceleration histories in two horizontal directions and θ is the rotation angle relative to the x-axis direction. Considering N_r original record each rotated to N_a rotation angles, which are distributed uniformly between 0 and 180 degrees, there exists N_a^{Nr} different possibilities for selecting N_r records each from a separate recording. In this regard, out of all possible selections, the structures are analyzed under 10^5 randomly selected sets of size 100 waveforms. Using the *Cloud Analysis*, the corresponding fragility functions are derived with the *Engineering Demand Parameter (EDP)* of the Maximum Inter-Story Drift Ratio (*MIDR*) at for three limit states (LS_{MIDR}). In two instances, Figures (1) and (2) illustrate the calculated functions for 3 and 9-story structures, respectively. In Figure 1, the functions corresponding to intensity measures *MIV*, $S_a(T_1)$, and *CAD* given LS_{MIDR} = 0.01 are respectively depicted in A, C, and E, and for the same IMs given LS_{MIDR} =0.04, they are shown in B, D, and F, respectively. Also, the *target fragility function* defined as the one derived from the set consisting of all records at all angles is shown with a thicker line. Details of the structure and records will be given later. With a similar procedure, the probability of exceeding LS_{MIDR} =0.04 corresponding to more significant damage has been drawn for similar *IMs* in B, D, and F, respectively.

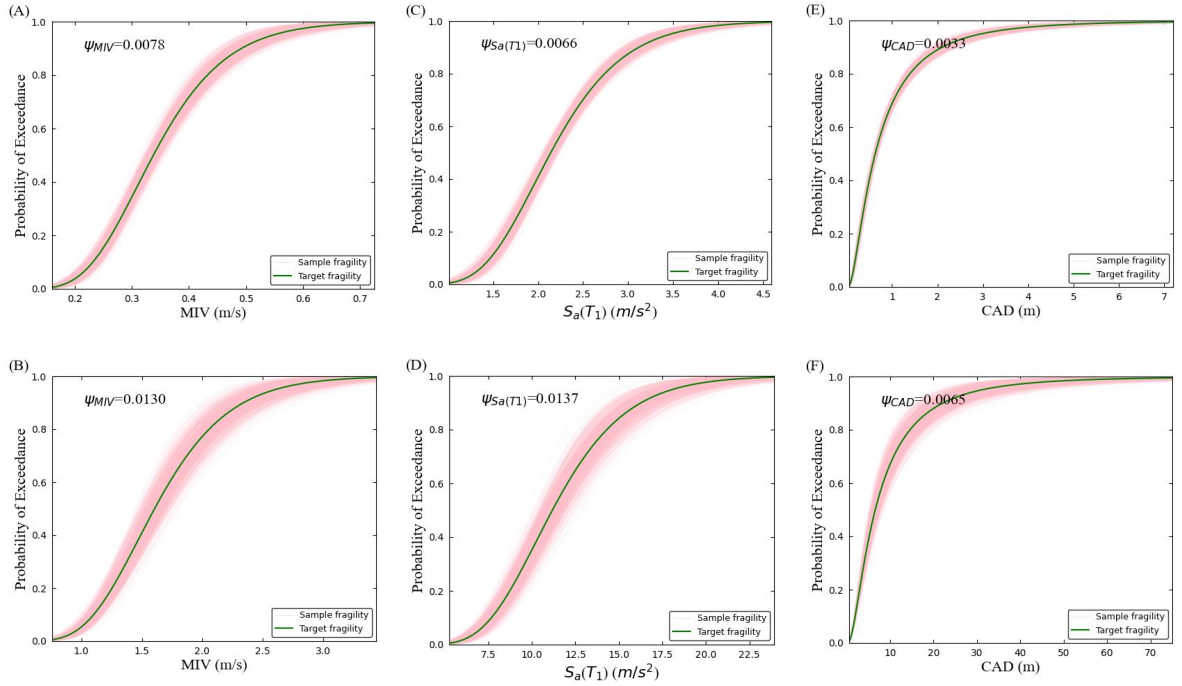

Figure (1): 3-Story: (A) LS_{MIDR}=0.01, IM=MIV- (B) LS_{MIDR}=0.04, IM=MIV- (C) LS_{MIDR}=0.01, IM=$S_a(T_1)$- (D) LS_{MIDR}=0.04, IM=$S_a(T_1)$- (E) LS_{MIDR}=0.01, IM=CAD- (F) LS_{MIDR}=0.04, IM=CAD.

As can be seen, the selection of different rotation angles can change the mean and standard deviation of the fragility functions significantly. For the sake of virtual comparison, the graphs are drawn for the *IM* levels associated with probabilities from 0.005 to 0.995. Among these cases, the lowest dispersion belongs to the *CAD* intensity measure and the highest one to the *MIV*. Moreover, in all cases, the level of variability increases at higher levels of nonlinearity. Similar trends also can be seen in Figure 2 in the case of the 9-story structure. These observations indicate the bias in the results of the probabilistic seismic assessment by ignoring the impact of rotation angle and signify the importance of *IM* selection and its direct impact in this regard. To quantify the mentioned effects, using the concept of relative entropy, the *Angular Efficiency* as a measure of this uncertainty is presented in Eq. 2:

$$\psi_{IM} = \frac{\sum_{i=1}^{N_{sample}} D_{kl,i}}{N_{sample}} \tag{2}$$

Where N_{sample} is the number of examined sample sets (i.e., fragility functions), which is 10^5 in this study. Although the sensitivity of angular efficiency of *IMs* on the sample size is not the same, the N_{sample} is chosen large enough to remove those effects. Also, $D_{kl,i}$ is defined as the relative entropy between the derivative of the fragility function associated with the i-th sample compared to the derivative of the target fragility as presented in Eq 3.

$$D_{kl,i} = \int_{-\infty}^{+\infty} p_i \ln \frac{p_i}{q} dIM \tag{3}$$

$$p_i = \frac{dP\left(EDP > LS_{EDP} \middle| IM, D_i\right)}{dIM} \tag{4}$$

$$q = \frac{dP\left(EDP > LS_{EDP} \middle| IM, D_{Total}\right)}{dIM} \tag{5}$$

where p_i and q are the derivatives of the sample fragility curve and the target fragility curve with respect to the Intensity Measure, respectively. D_i represents the i-th sample space and D_{Total} represents the total set of original records at different angles.

Relative entropy is shown to be a robust measure to characterize the variation between two fragility functions, capturing the alteration in their mean and dispersion. The arithmetic average assigns the same weight to every sample given the equal probability of different rotation angles for a record.

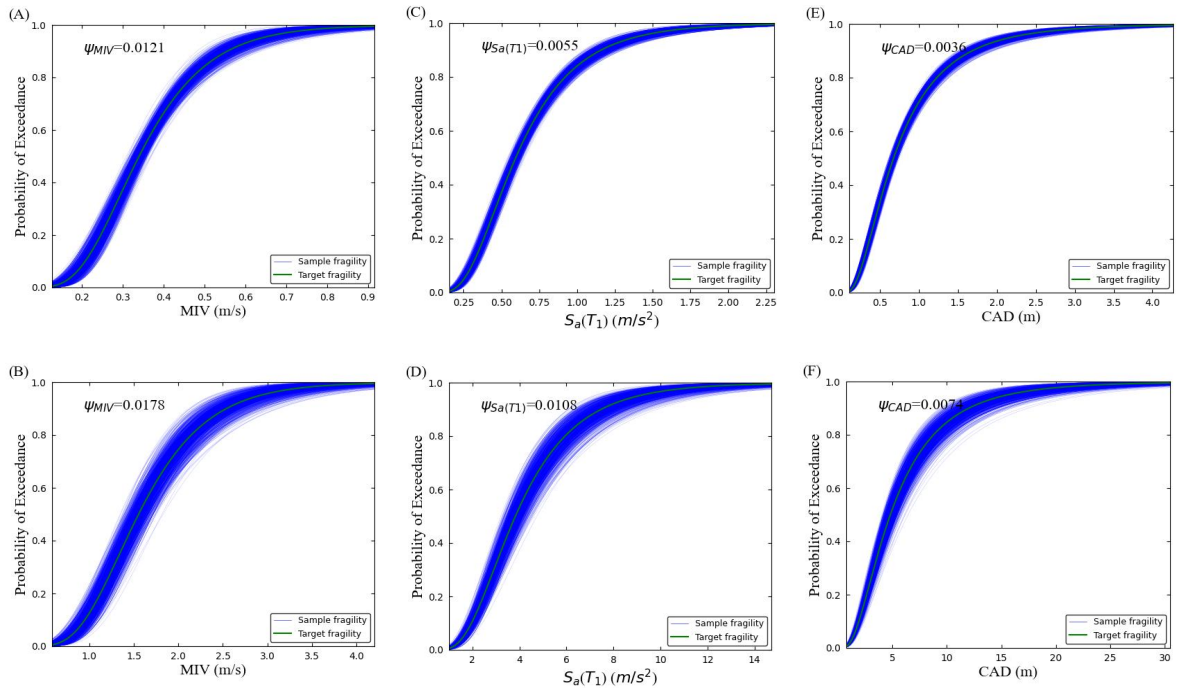

Figure (2): 9-Story: (A) LS_{MIDR}=0.01, IM=MIV- (B) LS_{MIDR}=0.04, IM=MIV- (C) LS_{MIDR}=0.01, IM=$S_a(T_1)$- (D) LS_{MIDR}=0.04, IM=$S_a(T_1)$- (E) LS_{MIDR}=0.01, IM=CAD- (F) LS_{MIDR}=0.04, IM=CAD.

3- Uncertainty of record to record

Record-to-record uncertainty is arguably the most widely studied source of seismic uncertainty. During the past two decades, many efforts have been made to introduce improved Intensity Measures to reduce the dispersion of the results, or in other words to increase efficiency. Also, many researchers tried to evaluate the performance of different *IMs* in the seismic assessment for various types of structures (Zaker Esteghamati, 2022). In the context of *Cloud Analysis* (Cornell et al., 2002), given a set of records, the standard deviation of the linear regression quantifies the dispersion of *EDP* values obtained from the nonlinear analysis of the structure determined using Eq. 6:

$$E\left[\ln EDP \middle| IM\right] = \ln \eta_{EDP|IM} = \ln a + b \ln IM \tag{6}$$

$$\beta_{\ln EDP|IM,NoC} = \sqrt{\frac{\sum_{k=1}^{N} (\ln(EDP_k) - \ln \eta_{EDP|IM_k})^2}{N-2}} \tag{7}$$

where EDP_k is the response of the structure under the k-th record, $\eta_{EDP|IM}$ is the estimated *EDP* at the level of *IM* obtained from the linear regression, and *N* is the number of analyses with non-collapse results. Every regression is conducted using 100 records, each of which is from a separate recording device with a random rotation angle. Thus, the dispersion of the regression merely pertains to the record-to-record, not the angle-to-angle variability. Eventually, the values of $\beta_{lnEDP|IM}$ are averaged among sets to come up with a unique value for an *EDP-IM* pair as presented in Eq. 8.

$$\bar{\beta}_{EDP|IM} = \frac{\sum_{i=1}^{N_{sample}} \beta_{\ln EDP|IM_i}}{N_{sample}} \tag{8}$$

4- Case-study buildings, ground motions and intensity measures

In this study, two 3- and 9-story steel structures from the *SAC* project are modeled and analyzed. The structures were designed to comply with the *UBC94* code for the city of Los Angeles, considering post-earthquake Northridge requirements. The periods of the structures at the first mode of vibration are 1.03 and 2.48 seconds, respectively. Non-linear modeling is carried out in *OpenSees*(McKenna et al., 2010), and its details can be found in (Gupta, 1999; Shargh et al., 2023).

Table (1): The suite of strong ground motion records from the New Zealand database.

Record	M_w	R_{rup}(km)	Record	M_w	R_{rup}(km)
20110613_022049_GODS	5.99	3.62	20110221_235142_HVSC	6.19	4.19
20110613_022049_PARS	5.99	3.63	20100903_163541_HORC	7.08	0.84
20161113_110317_KEKS_20	7.85	2.96	20110221_235142_CBGS	6.19	5.94
20161113_110259_WTMC_20	7.85	1.47	20110221_235142_LPOC	6.19	7.07
20100903_163541_GDLC	7.08	1.34	20100903_163541_CHHC	7.08	16.47

A set of 100 original ground motions is employed including 90 two-component ground motions from the *PEER* (Seyhan et al., 2014) (refer to (Shargh et al., 2023) for details), and 10 from the New Zealand

database (Van Houtte et al., 2017) (Table 1). As mentioned previously, every pair of recordings is rotated to 10 angles with equal intervals of 18 degrees between 0 and 180 degrees from x orientation, and in total, each structure is subjected to 1000 nonlinear time history analyses. Moreover, a set of 41 Intensity Measures is selected to investigate and compare their performance through the developed method (Table 2). (Chen et al., 2023; Heresi et al., 2021; Moehle et al., 2004; Zengin et al., 2020)

6- Results

In Figure 3, the resultant $\beta_{EDP|IM}$ and ψ_{IM} are indicated as the measures of *R-to-R efficiency* and *angular efficiency*, respectively. Both measures are calculated for all the intensity measures listed in Table 1, for two structures and two maximum LS_{MIDR}= 0.01 and 0.04, derived from 10^5 sample sets and fragility assessments. It should be noted that, for the sake of demonstration, in the case of B and D only the ψ_{IM} values lower than 0.03 are displayed to conduct a better comparison based on the limit states, rendering the results of the two intensity measures invisible. As expected, for both structures, the values of ψ_{IM} increase due to the higher nonlinearity of the limit state, while *efficiency* values are independent of the considered LS_{MIDR}.

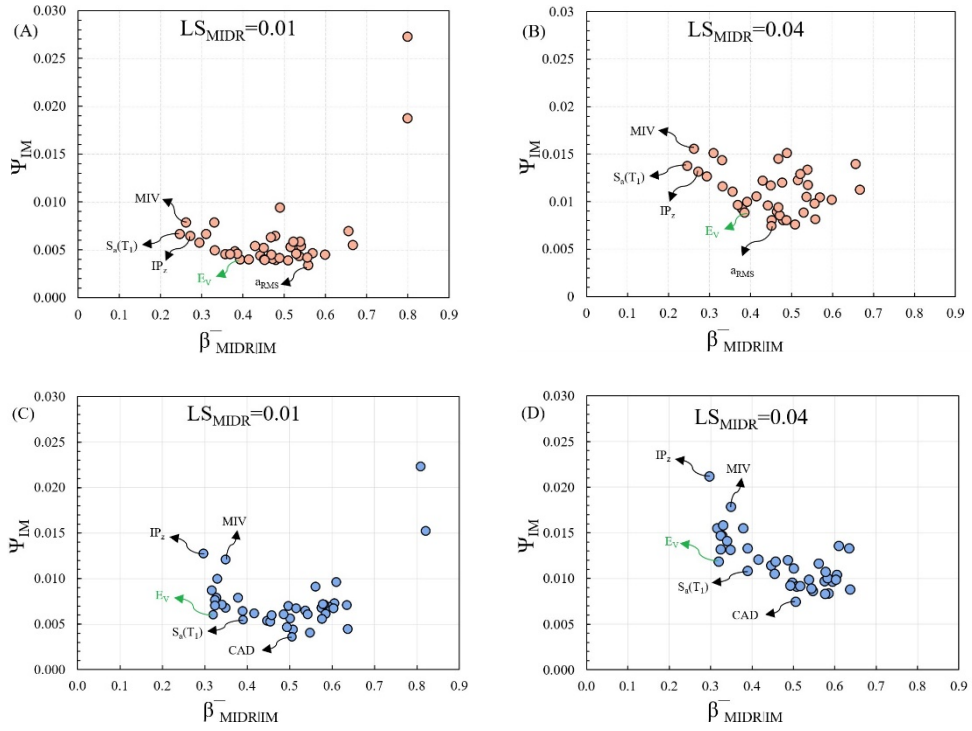

Figure 3): Values of $\beta_{EDP|IM}$ and ψ_{IM} for (A) 3-Story building, LS_{MIDR}=0.01 (B) 3-Story building, LS_{MIDR}=0.04 (C) 9-Story building, LS_{MIDR}=0.01 (D) 9-Story building, LS_{MIDR}=0.04

It is readily observable that the most optimal intensity measures in terms of *R-to-R efficiency* are not necessarily the best in terms of *angular efficiency*. Thus, in the *IM* selection phase, intensive focus on reducing the dispersion caused by the *R-to-R* variability may increase the induced uncertainty caused by the *A-to-A* variability. Therefore, it can be inferred that the development of new intensity measures requires considering the uncertainty of both sources simultaneously. Some of the best measures of intensity are annotated in the Figure 3. Regardless of the considered limit state, $S_a(T_1)$ and IP_z measures

have the lowest $\beta_{EDP|IM}$ in the 3 and 9-story structures, respectively. However, their associated ψ_{IM} values are significantly large compared to other *IMs* for each structure, listing them among the worst measures in terms of angular efficiency.

Table (2): 41 of ground motion intensity measures

$1.PGA = \max_0^t\left(\lvert\ddot{u}_g(t)\rvert\right)$	$11.MID = \max\left(\left\lvert\int^{t_{0,i+1}} \dot{u}_g(t)dt\right\rvert\right)$	$21.a_{RMS} = \sqrt{E_a}$	$30.d_{RMS} = \sqrt{E_d}$
$2.SMA = 3rd_0^t\left(\lvert\ddot{u}_g(t)\rvert\right)$ Butterworth digital lowpass, Low cut of frequency=9 Hz, Order=4	$12.E_v = \int_{t_{5\%}}^{t_{95\%}}\left[\dot{u}_g(t)\right]^2 dt$	$22.I_c = a_{RMS}^{3/2}.t_D^{1/2}$	$31.I_d = PGD.t_D^{1/3}$
$3.EDA = \max_0^t\left(\lvert\ddot{u}_{g,f}(t)\rvert\right)$	$13.CAD = \int^{t_{95\%}}\lvert\dot{u}_g(t)\rvert dt$	$23.I_a = PGA.t_D^{1/3}$	$32.IM = \frac{PGD^2}{}$
$4.SMA_f = 3rd_0^t\left(\lvert\ddot{u}_{g,f}(t)\rvert\right)$ The acceleration level below which 95% of .the total Arias intensity is contained	$14.S_a(T_1)$	$24.P_D = \frac{\pi}{2g}.\frac{E_a}{N^2}$	$33.DI = \frac{E_d}{PGD}$
$5.MIV = \max_i\left(\left\lvert\int_{t_{0,i}}^{t_{0,i+1}} \ddot{u}_g(t)dt\right\rvert\right)$	$15.Ld_v = \sum_{i=1}^{n}\left(\sqrt{\Delta t^2 + \Delta\dot{u}_{g,i}^2}\right)$	$25.v_{RMS} = \sqrt{\frac{E_v}{t_D}}$	$34.Lm_a = PGA.T_m^2$
$6.E_a = \int^{t_{95\%}}\left[\ddot{u}_g(t)\right]^2 dt$	$16.PGD = \max_0^t\left(\lvert u_g(t)\rvert\right)$	$26.I_v = PGV^{2/3}.t_D^{1/3}$	$35.Lm_v = PGV.T_m$
$7.CAV = \int^{t_{95\%}}\lvert\ddot{u}_g(t)\rvert dt$	$17.SMD = 3rd_0^t\left(\lvert u_g(t)\rvert\right)$ Butterworth digital lowpass, Low cut of frequency=9 Hz, Order=4	$27.I_f = PGV.t_D^{1/4}$	$36.I_h = \tau_c.PGD$
$8.TD = \sum^{t_{end}} H\left[\ddot{u}_g(t) - 0.05g\right]$	$18.E_d = \int^{t_{95\%}}\left[u_g(t)\right]^2 dt$	$28.I_{\Delta-PGV} = PGV^{3/2}.t_D^{1/2}$	$37.R_{PGV-PGA} = \frac{PGV}{PGA}$
$9.PGV = \max_0^t\left(\lvert\dot{u}_g(t)\rvert\right)$	$19.CAI = \int^{t_{95\%}}\lvert u_g(t)\rvert dt$	$29.VI = \frac{E_v}{}$	$38.R = \frac{PGV^2}{}$
$10.SMV = 3rd_0^t\left(\lvert\dot{u}_g(t)\rvert\right)$ Butterworth digital lowpass, Low cut of frequency=9 Hz, Order=4	$20.T_m = \frac{\sum_{i=1}^{N}\frac{C_i^2}{f_i}}{}, 0.25 \le f_i \le 20\,Hz$	$39.IP = \max_{\forall t<t_{end}-0.5T_1}\left(\frac{\int_t^{t+0.5T_1}\dot{u}_{g,f}^2(t)dt}{0.5T_1}\right)$ Butterworth digital bandpass, Low cut of frequency=1/(3T₁) Hz, high cut of frequency=1/(0.2T₁) Hz, Order=4	
$40.\ h = \sum_i \frac{E(f_i)}{f}\left[\frac{0.3}{T_1} \le f_i \le 15\,Hz,\ \Delta f_i = 0.05\ Hz\right]$			
$41.\ FIV3 = max\left\{\left(V_{s,max1} + V_{s,max2} + V_{s,max3}\right), \lvert V_{s,min1} + V_{s,min2} + V_{s,min3}\rvert\right\}$ $V_s(t) = \int_t^{t+0.7T_1}\ddot{u}_{g,f}(t)dt, \forall t < t_{end} - 0.7T_1$ Butterworth digital lowpass, Low cut of frequency=1 Hz, Order=2			

On the other hand, a_{RMS} for 3- and *CAD* for 9-story building had the lowest values of ψ_{IM}, which means they led to the lowest dispersion in the calculated fragility functions on average among all *IMs*. However, their performance in terms of *R-to-R efficiency* is low compared to other measures. Hence, when it comes to selecting a proper intensity measure in this context, there exists an indispensable trade-off between the competency of an *IM* to reduce the involved uncertainty due to *R-to-R* and *A-to-A* variability. This observation indicates the need for simultaneous consideration of both types of randomness for evaluation and selection of a versatile *IM*, which can also depend on the importance of each in different conditions. This type of decision-making has been intensively studied in the literature, mostly regarding the multi-objective optimization problem. However, in this study, the Euclidean distance of each *IM* to the origin is adopted as the decision policy, leading to an *IM* with proportionate competency in reducing both types of randomness. In this regard, E_v has shown to be versatile in estimating *MIDR* values and lowering the dispersion among the resultant fragility functions regarding the impact of rotation angle.

7- References

Chen, G., Yang, J., Liu, Y., Kitahara, T., & Beer, M. (2023). An energy-frequency parameter for earthquake ground motion intensity measure. *Earthquake Engineering & Structural Dynamics*, *52*(2), 271–284.

Cornell, C. A., Jalayer, F., Hamburger, R. O., & Foutch, D. A. (2002). Probabilistic basis for 2000 SAC federal emergency management agency steel moment frame guidelines. *Journal of Structural Engineering*, *128*(4), 526–533.

Gupta, A. (1999). *Seismic demands for performance evaluation of steel moment resisting frame structures*. Stanford University.

Heresi, P., & Miranda, E. (2021). Intensity measures for regional seismic risk assessment of low-rise wood-frame residential construction. *Journal of Structural Engineering*, *147*(1), 4020287.

Luco, N., & Cornell, C. A. (2007). Structure-specific scalar intensity measures for near-source and ordinary earthquake ground motions. *Earthquake Spectra*, *23*(2), 357–392.

McKenna, F., Scott, M. H., & Fenves, G. L. (2010). Nonlinear finite-element analysis software architecture using object composition. *Journal of Computing in Civil Engineering*, *24*(1), 95–107.

Moehle, J., & Deierlein, G. G. (2004). A framework methodology for performance-based earthquake engineering. *13th World Conference on Earthquake Engineering*, *679*.

Seyhan, E., Stewart, J. P., Ancheta, T. D., Darragh, R. B., & Graves, R. W. (2014). NGA-West2 site database. *Earthquake Spectra*, *30*(3), 1007–1024.

Shargh, G. B., & Barati, R. (2023). Probabilistic assessment of ground motion rotation impact on seismic performance of structures. *Engineering Structures*, *292*, 116383.

Shargh, G. B., Barati, R., & Brown, N. (2024). ANGULAR EFFICIENCY OF INTENSITY MEASURES. *18th World Conference on Earthquake Engineering* (expected).

Van Houtte, C., Bannister, S., Holden, C., Bourguignon, S., & McVerry, G. (2017). The New Zealand strong motion database. *Bulletin of the New Zealand Society for Earthquake Engineering*, *50*(1), 1–20.

Zaker Esteghamati, M. (2022). A Holistic Review of GM/IM Selection Methods from a Structural Performance-Based Perspective. *Sustainability*, *14*(20), 12994.

Zengin, E., & Abrahamson, N. A. (2020). A vector-valued intensity measure for near-fault ground motions. *Earthquake Engineering & Structural Dynamics*, *49*(7), 716–734.